



This is a repository copy of *Cavity-enhanced excitation of a quantum dot in the picosecond regime*.

White Rose Research Online URL for this paper:

<https://eprints.whiterose.ac.uk/203505/>

Version: Published Version

Article:

Javadi, A. orcid.org/0000-0002-8833-0738, Tomm, N., Antoniadis, N.O. et al. (6 more authors) (2023) Cavity-enhanced excitation of a quantum dot in the picosecond regime. *New Journal of Physics*, 25. 093027. ISSN 1367-2630

<https://doi.org/10.1088/1367-2630/acf33b>

Reuse

This article is distributed under the terms of the Creative Commons Attribution (CC BY) licence. This licence allows you to distribute, remix, tweak, and build upon the work, even commercially, as long as you credit the authors for the original work. More information and the full terms of the licence here:

<https://creativecommons.org/licenses/>

Takedown

If you consider content in White Rose Research Online to be in breach of UK law, please notify us by emailing eprints@whiterose.ac.uk including the URL of the record and the reason for the withdrawal request.



eprints@whiterose.ac.uk
<https://eprints.whiterose.ac.uk/>

PAPER • OPEN ACCESS

Cavity-enhanced excitation of a quantum dot in the picosecond regime

To cite this article: Alisa Javadi *et al* 2023 *New J. Phys.* **25** 093027

View the [article online](#) for updates and enhancements.

You may also like

- [Predator–prey survival pressure is sufficient to evolve swarming behaviors](#)
Jianan Li, Liang Li and Shiyu Zhao
- [Theory of a filament initiated nitrogen laser](#)
Daniil Kartashov, Skirmantas Ališauskas, Audrius Pugžlys et al.
- [Plasmonic superradiance of two emitters near a metal nanorod](#)
I E Protsenko, A V Uskov, Xue-Wen Chen et al.



PAPER

Cavity-enhanced excitation of a quantum dot in the picosecond regime

OPEN ACCESS

RECEIVED
27 January 2023REVISED
4 August 2023ACCEPTED FOR PUBLICATION
23 August 2023PUBLISHED
13 September 2023Original Content from
this work may be used
under the terms of the
[Creative Commons
Attribution 4.0 licence](https://creativecommons.org/licenses/by/4.0/).Any further distribution
of this work must
maintain attribution to
the author(s) and the title
of the work, journal
citation and DOI.Alisa Javadi^{1,*} , Natasha Tomm¹ , Nadia O Antoniadis¹ , Alistair J Brash² , Rüdiger Schott³,
Sascha R Valentin³, Andreas D Wieck³ , Arne Ludwig³  and Richard J Warburton¹ ¹ Department of Physics, University of Basel, Klingelbergstrasse 82, CH-4056 Basel, Switzerland² Department of Physics and Astronomy, University of Sheffield, Sheffield S3 7RH, United Kingdom³ Lehrstuhl für Angewandte Festkörperphysik, Ruhr-Universität Bochum, D-44780 Bochum, Germany

* Author to whom any correspondence should be addressed.

E-mail: alisa.javadi@gmail.com**Keywords:** single-photon source, quantum dot, microcavity, quantum optics, exciton-phonon coupling, coherent control

Abstract

A major challenge in generating single photons with a single emitter is to excite the emitter while avoiding laser leakage into the collection path. Ideally, any scheme to suppress this leakage should not result in a loss in the efficiency of the single-photon source. Here, we investigate a scheme in which a single emitter, a semiconductor quantum dot, is embedded in a microcavity. The scheme exploits the splitting of the cavity mode into two orthogonally-polarised modes: one mode is used for excitation, the other for collection. By linking the experiment to theory, we show that the best population inversion is achieved with a laser pulse detuned from the quantum emitter. The Rabi oscillations exhibit an unusual dependence on pulse power. Our theory describes them quantitatively, enabling us to determine the absolute population inversion. By comparing the experimental results with our theoretical model, we determine a population inversion of $98^{+1\%}_{-5\%}$ for optimal laser detuning. The Rabi oscillations depend on the sign of the laser-pulse detuning, a phenomenon arising from the non-trivial effect of phonons on the exciton dynamics. The exciton-phonon interaction is included in the theory and gives excellent agreement with all the experimental results.

1. Introduction

Quantum emitters efficiently interfaced with optical cavities represent primary components in photonic quantum technologies. They are used for generating quantum states of light such as single photons and entangled states. The generation efficiency requirement is strict, with many proposals requiring efficiencies higher than 90% [1, 2]. Generating photonic quantum states requires coherent control over the quantum emitter, which is often carried out using fast laser pulses. The main challenges are to ensure that the laser pulse results in occupation of the upper level with near-unity probability and that laser light does not enter the collection mode. Another major complication for solid-state quantum emitters is the interaction with the environmental degrees of freedom, in particular the acoustic phonons [3, 4].

Several approaches have been developed to separate the excitation pulse from the generated photons. One method excites the emitter via non-cavity modes that have a propagation direction perpendicular to the cavity axis, a scheme often used to generate photons from atoms and ions [5, 6]. In the solid-state domain, non-resonant excitation schemes, such as a phonon-assisted mechanism [7–10], allow for spectral filtering of the laser pulse. However, the essential spectral filtering unavoidably reduces the efficiency of the source. Additionally, phonon-assisted schemes require large pulse areas [8]. The pulse area can be reduced to the minimum, π , by exciting the quantum emitter resonantly. In such schemes, the collection and excitation modes have a different spatial [11] or polarization degree-of-freedom [12]. Avoiding losses is challenging. For instance, the cross-polarized scheme can result in the loss of 50% of the generated photons.

In many cases, the cavity mode splits into two modes with orthogonal polarization, a consequence of weak birefringence either in the mirrors or in the solid-state host. This mode structure offers a solution to the excitation-collection challenge. One cavity-mode, resonant with the quantum emitter, is used for collection; the other cavity-mode is used for excitation [13]. Furthermore, if the quantum emitter has a circularly-polarized optical dipole-moment, photon loss can be minimized in the cross-polarized detection scheme: the emitter is coupled with high efficiency to the collection mode, and with small efficiency to the excitation mode [13]. The scheme was originally developed for quantum dots (QDs) in semiconductor micropillars, for which the cavity mode-splitting is induced by an elliptical pillar cross-section [13]. It was subsequently employed in a QD-in-open-cavity device [14]. In this case, the mode-splitting arises from birefringence in the semiconductor heterostructure, and it can be tuned via the electro-optic [15] and photo-elastic effects [16].

Here, we probe both experimentally and theoretically the cavity-based excitation-collection scheme using a QD coupled to a one-sided open-microcavity, figure 1(a). The experiment explores the dependence on both laser detuning and pulse power. The theoretical model describes the effect of the cavity on the excitation pulse. It also includes the exciton-phonon interaction. The model accurately describes the experimental results allowing us to quantify the probability of exciton creation (equivalently, the population inversion), to understand the unusual Rabi oscillations, and to predict the behaviour as a function of cavity-mode splitting.

2. Cavity-mediated excitation of a two-level system

We initially consider pulsed excitation of a two-level system (TLS) in the ideal limit, where decay and dephasing processes are absent, and for pulse durations significantly shorter than the lifetime of the emitter. In the case of a transform-limited pulse, a resonant pulse drives the TLS around the Bloch-sphere, inverting its population from the ground state $|g\rangle$ to the excited state $|e\rangle$, black dots in figure 1(b). On increasing the pulse area, the population coherently rotates around the Bloch-sphere, giving rise to the well-known Rabi-oscillations, gray line in figure 1(c).

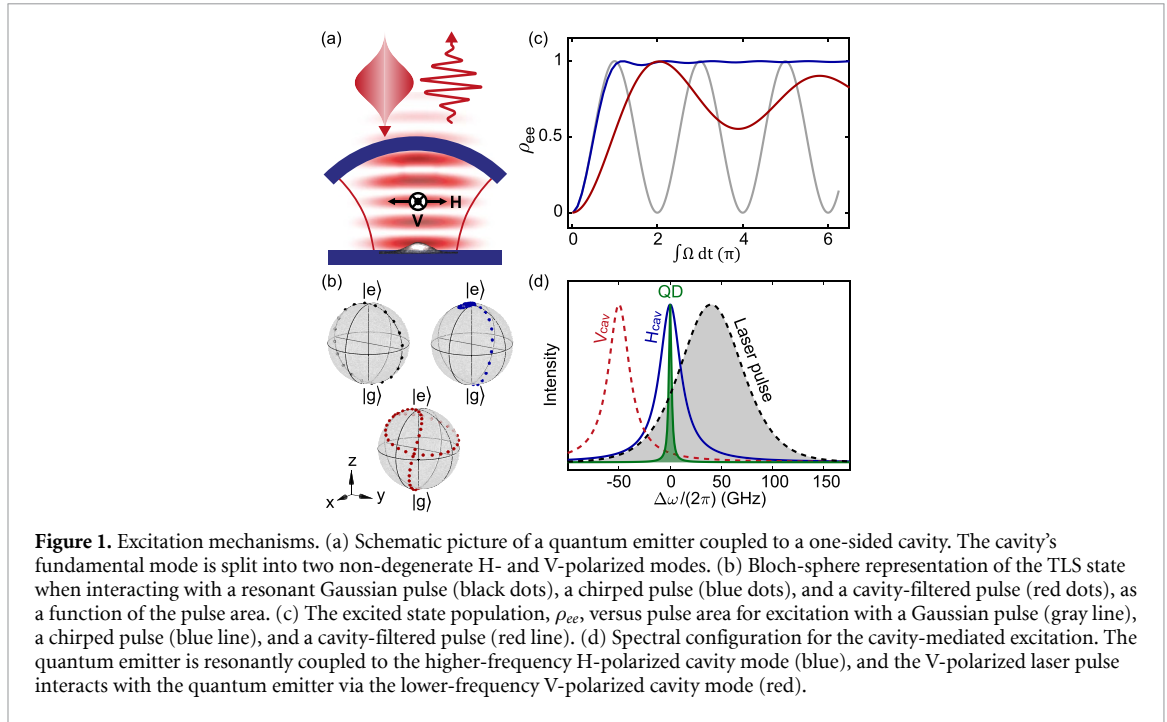
Another well-known case is the dynamics of a TLS under excitation with a strongly chirped pulse, known as rapid adiabatic passage [17, 18], where the excitation frequency sweeps through the resonance of the TLS during the pulse. The TLS interacts with different frequency components present in the pulse at different instances in time, leading to a different trajectory on the Bloch-sphere, blue dots figure 1(b). Starting at the south pole of the Bloch sphere, the TLS population oscillates around the north pole of the Bloch sphere at the end of the pulse, making the excited state population insensitive to the pulse area, figure 1(c).

In the case of cavity-mediated excitation with a detuned pulse, a Gaussian-shaped pulse is convoluted with the time-response of the cavity itself. Effectively, the cavity acts as a dispersive filter, altering the spectral profile of the pulse such that it can no longer be described by a Gaussian profile in the frequency domain. Figure 1(d) illustrates the spectral configuration of the original laser pulse and the cavity modes. The TLS is resonant with the higher-frequency cavity mode (H-polarized), and the laser pulse is launched via the lower-frequency (V-polarized) cavity mode. The red curves in figures 1(b) and (c) show the evolution of the TLS as a function of the input pulse area. A full population in the excited state can be obtained, but population inversion is incomplete at higher pulse areas. At high pulse areas, the excited state population converges to a constant value lying between 0 and 100%, depending on the detuning. This behaviour at high pulse areas significantly differs from the other two excitation mechanisms. Note that the detuning between the excitation cavity and the laser pulse plays a vital role in this scheme. Tuning the laser into resonance with the excitation cavity would result in the TLS experiencing a simple detuned pulse, leading to a limited population inversion.

3. Experimental results

We use a QD in an open microcavity [14] to investigate the cavity-mediated excitation scheme. The QD is occupied with a single hole such that optical excitation creates a positively-charged trion. The cavity comprises a 'top' dielectric mirror with a reflectivity of 99% and a 'bottom' semiconductor mirror with a reflectivity of 99.97%. A QD layer is grown on the semiconductor mirror; the QD layer is embedded in the intrinsic region of a p-i-n diode: the diode facilitates control of the QD charge (via Coulomb blockade) and also fine-tuning of the optical resonance (via the dc Stark effect).

The cavity has a line width of 25 GHz and a mode volume of $1 \mu\text{m}^3$ at the operating wavelength (920 nm). A QD positioned at the centre of the cavity experiences a Purcell enhancement of ~ 10 (resulting radiative lifetime ~ 45 ps) on resonance with the cavity. The cavity hosts two modes with orthogonal polarization and a mode-splitting of 50 GHz. The laser pulses have a temporal width (intensity full-width at half maximum) between 3.6 and 5.0 ps.

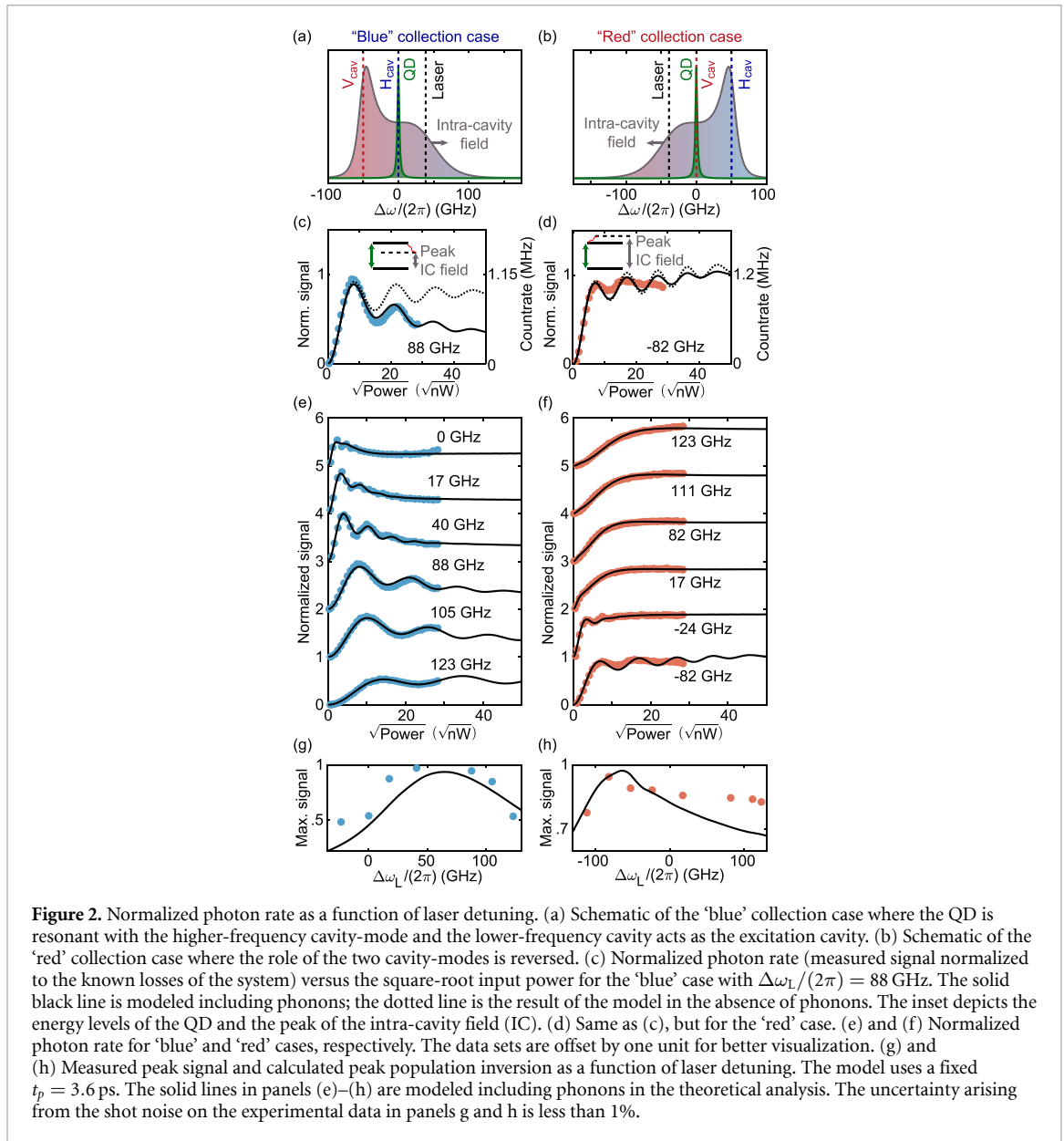


We use the polarization of the excitation laser to select the excitation cavity mode. Figure 1(d) shows the case where the QD is on resonance with the higher-frequency (H-polarized) mode and the laser is launched through the lower-frequency (V-polarized) mode, the ‘blue’ collection case. Figure 2(a) shows the calculated intra-cavity field in this configuration. As evident from the spectrum, the intra-cavity field exhibits a strong peak below the QD resonance. Figure 2(b) shows the spectrum in the inverted case, the ‘red’ collection case: the QD is on resonance with the lower-frequency (V-polarized) mode and the laser is launched through the higher-frequency (H-polarized) mode.

We first present experimental results on the ‘blue’ collection case. Figure 2(c) shows the normalized single-photon rate as a function of the input laser power. The laser is detuned from the QD by $\Delta\omega_L/(2\pi) = 88$ GHz ($\Delta\omega_L = \omega_L - \omega_{QD}$). The detected single-photon rate exhibits the expected oscillatory behaviour along with strong damping as the laser power is increased. The damping arises from the interaction between the QD exciton, the red-detuned components of the intra-cavity field, and the phonons in the environment of the QD. Specifically, the damping process involves the QD decaying by emitting a photon on resonance with the intra-cavity peak and a phonon, as illustrated in the inset of figure 2(c). The process is enhanced by the large amplitude of the intra-cavity field, and leading to more pronounced damping at higher laser powers. Processes of this nature have already been observed in pump-probe experiments [19]. The theoretical model presented in section 4 accurately captures these details, as depicted by the solid lines in figure 2(c).

A crucial metric is the population inversion, the probability of creating an exciton in the QD following pulsed excitation. The probability of creating a photon in the collection cavity-mode is $\eta_c = \beta_c \pi_e$ where π_e stands for the population inversion, and β_c the probability that an exciton creates a photon in the collection cavity-mode. It is hard to access π_e directly in an experiment. However, β_c and the other factors which determine the measured photon flux [14] remain constant with respect to laser power. This allows π_e to be determined by fitting the measured flux–power curve to the theoretical model. The excellent agreement between theory and experiment allows us to deduce that we achieve a maximum population inversion of $\pi_e = 96\%_{-7\%}^{+1\%}$ in this experiment. The theory also allows us to quantify the exact role of phonons—the dashed line in figure 2(c) shows the theory with the exciton-phonon interaction turned off. At low powers, phonons only slightly limit the population inversion ($99\% \rightarrow 96\%$), but they have a more significant effect at high powers.

We turn to the ‘red’ collection case, a scheme mirrored in frequency with respect to the ‘blue’ case. Figure 2(d) shows the normalized single-photon rate as a function of the input laser power with $\Delta\omega_L/(2\pi) = -82$ GHz. Interestingly, the strong damping disappears in this case. This is due to the fact that a phonon-mediated process is suppressed: the peak of the intra-cavity field lies at a higher frequency than the QD resonance, such that phonon-mediated depopulation of the excited state would require absorption of a phonon, which is suppressed at the temperature of the experiment (4.2 K), due to the low thermal



population of the phonon bath. The symmetry breaking in the system’s evolution, ‘red’ with respect to ‘blue’, is strong evidence for the role of phonons in the system dynamics [20, 21]. Similar to the ‘blue’ case, the theoretical model reproduces the experimental results very convincingly. At higher powers, the theoretical curve slightly overshoots unity. This behaviour is attributed to two-photon emission processes: the QD emits one photon during the excitation pulse and is subsequently re-excited by the same pulse such that a second photon is created [22, 23].

Figure 2(e) and f show the measured normalized photon rates for different laser detunings ($\Delta\omega_L/(2\pi)$) in the ‘blue’ and ‘red’ collection cases, respectively. In the ‘blue’ collection cases (figure 2(e)), Rabi oscillations along with phonon-induced damping are evident. The peak population inversion exceeds 90% for $\Delta\omega_L/(2\pi)$ between 40 GHz and 100 GHz. At resonance and for negative detunings, $\Delta\omega_L \leq 0$, the peak population inversion decreases drastically. On the other hand, for the ‘red’ collection cases (figure 2(f)), the oscillatory behaviour is less pronounced and only present when the laser is red-detuned, $\Delta\omega_L \leq 0$. Remarkably, the population inversion can still be close to unity for $\Delta\omega_L \geq 0$. A phonon-assisted excitation of the QD can describe this: in this scenario, the intra-cavity field lies at higher frequencies than the QD transition such that a laser photon can be converted to a QD-exciton and a phonon [7, 21].

Figures 2(g) and (h) illustrate the highest measured photon rates as a function of the excitation frequency for the ‘red’ and ‘blue’ schemes (data in figures 2(e) and (f), respectively). In both cases, the maximum is achieved for a detuned pulse.

Figure 4 shows the normalized photon count rate as a function of the excitation power and the frequency of the cavity modes for a fixed laser wavelength. Figure 4(a) corresponds to the ‘blue’ collection case where $\Delta\omega_L/(2\pi) = 35$ GHz and $t_p = 4.4$ ps. At resonance, clear damping of the Rabi rotations is observed as the excitation pulse area increases, in agreement with the results presented in figure 4(b). A different profile is observed in the ‘red’ collection case, when the QD emits photons into the lower-frequency V-polarized cavity mode, as seen in figure 4(c), where $\Delta\omega_L/(2\pi) = -23.57$ GHz and $t_p = 3.6$ ps. Here, at resonance, the normalized photon rate tends to plateau as the excitation pulse area increases. Both the experimental data and the model show a clear asymmetry between excitation via a red- or blue-detuned cavity mode. This asymmetry is consistent with the data presented in figure 2.

4. Theoretical treatment

The interaction between a TLS coupled to the collection cavity and a driving electric field is described with the standard Hamiltonian:

$$\hat{H} = \hbar \Delta\omega_c \hat{a}_c^\dagger \hat{a}_c + \hbar g (\hat{a}_c^\dagger \hat{\sigma}_- + \hat{a}_c \hat{\sigma}_+) + \hbar \left(\overline{E(t)} \cdot \vec{\mu} \right) (e^{i\omega_0 t} \hat{\sigma}_+ + e^{-i\omega_0 t} \hat{\sigma}_-). \quad (1)$$

The Hamiltonian is in the rotating frame of the TLS. $\omega_0/(2\pi)$ is the resonance frequency of the TLS, $\Delta\omega_c/(2\pi)$ the frequency detuning between the collection cavity-mode and the TLS ($\Delta\omega_c = \omega_c - \omega_0$), and \hat{a}_c^\dagger the photon creation operator for the collection cavity. $\overline{E(t)}$ is the intra-cavity field driving the TLS. The leakage through the top mirror is modeled using the Lindblad operator $\hat{\mathcal{L}} = \sqrt{\kappa} \hat{a}_c$.

The laser interacts with the TLS via the second cavity mode, the excitation mode, with resonance frequency $\omega_e/(2\pi)$. The intra-cavity field is a convolution of the input pulse and the impulse response of the cavity mode. The impulse response of a cavity is $h(\tau) = e^{-\frac{\kappa\tau}{2}} \cos(\omega_e \tau) \Theta(\tau)$, where $\kappa/(2\pi)$ is the linewidth of the cavity mode. Assuming an input field $E_0(t) = (\pi t_p)^{-1} \text{sech}(t/t_p) \cos(\omega_L t)$, typical of a mode-locked laser, the intra-cavity field is:

$$\overline{E(t)} = \frac{\kappa e^{i\omega_L t} \text{sech}(t/t_p)}{2\pi j_m} \times {}_2F_1(1, 1, 1 + j_m/2, \text{sech}(t/t_p)/2) + \text{c.c.}, \quad (2)$$

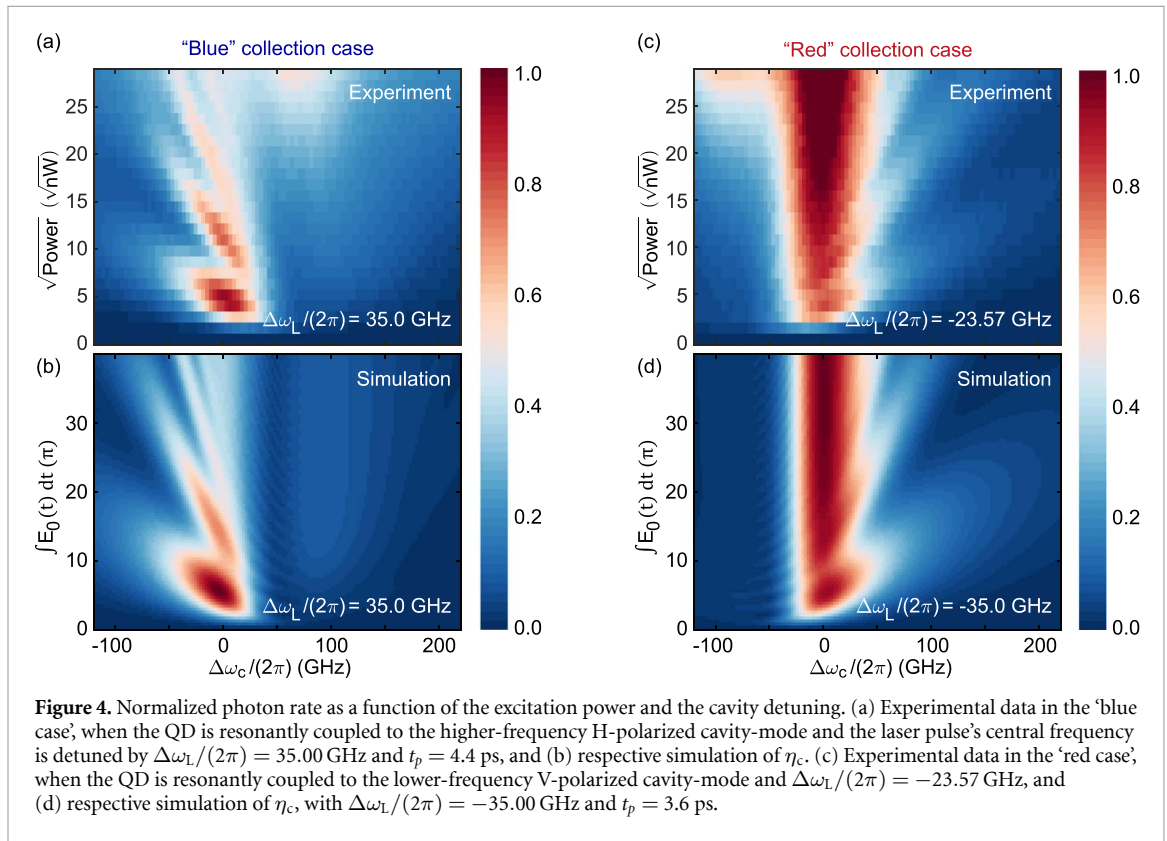
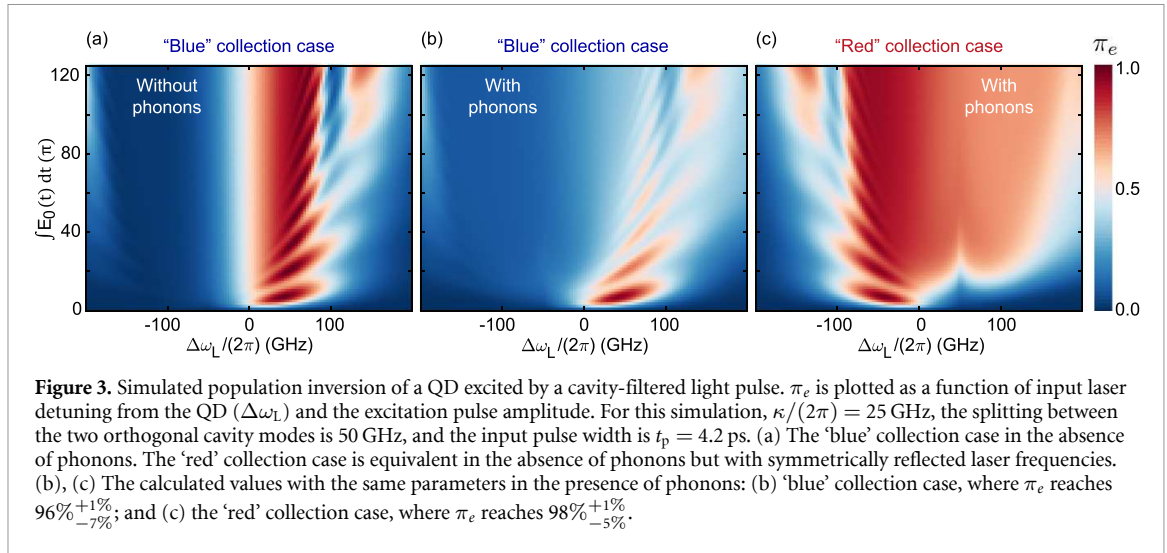
where $j_m = 1 - (i\Delta\omega_{EL} - \kappa/2)t_p$, $\omega_L/(2\pi)$ is the centre frequency of the laser, t_p the input pulse width, $\Delta\omega_{EL}/(2\pi)$ the detuning between the laser and the excitation cavity mode, and ${}_2F_1$ Gauss’s hypergeometric function. We plug equation (2) into equation (1) and apply the standard rotating-wave approximation.

Phonons play a significant role in the dynamics of a QD as the instantaneous Rabi frequency can be as high as several terahertz at which the exciton-phonon coupling is strongest. Assuming weak coupling of the exciton to the environment, one can include the effect of phonons on the TLS dynamics using the Bloch–Redfield master equation [24–26].

We use the Python package Qutip [27, 28] to set up and solve the equations of motion based on the Hamiltonian in equation (1). Finally, the photon creation probability in the collection mode (η_c) is calculated as $\beta_c \pi_e$ with $\pi_e = \int \kappa \langle \hat{a}_c^\dagger \hat{a}_c \rangle dt$ and $\beta_c = \frac{F_p(\omega_c)}{F_p(\omega_c) + F_p(\omega_e) + 1}$, the probability of the QD exciton creating a photon in the collection cavity mode. Note that $\int \kappa \langle \hat{a}_c^\dagger \hat{a}_c \rangle dt$ is the number of photons generated by the excitation pulse and in principle can exceed one (via multiple excitations of the TLS by one pulse). However, in the regime explored here (pulse duration much less than radiative decay time), $\int \kappa \langle \hat{a}_c^\dagger \hat{a}_c \rangle dt$ follows the population of the TLS upper-state very closely and we choose to describe it with ‘population inversion’.

To extract numerical results, we take the exciton-phonon coupling as described in [29], assuming a spherically symmetric wavefunction for both electrons and holes ($\psi \propto e^{-r^2/r_0^2}$). Our model matches the experimental data very well for an electron radius of 5.9 nm and a hole radius of 3.6 nm. In the calculations, $\kappa/(2\pi) = 25$ GHz and the cavity mode-splitting is 50 GHz as extracted from earlier measurements [14]. The pulse width lies between 3.6 ps and 5.0 ps.

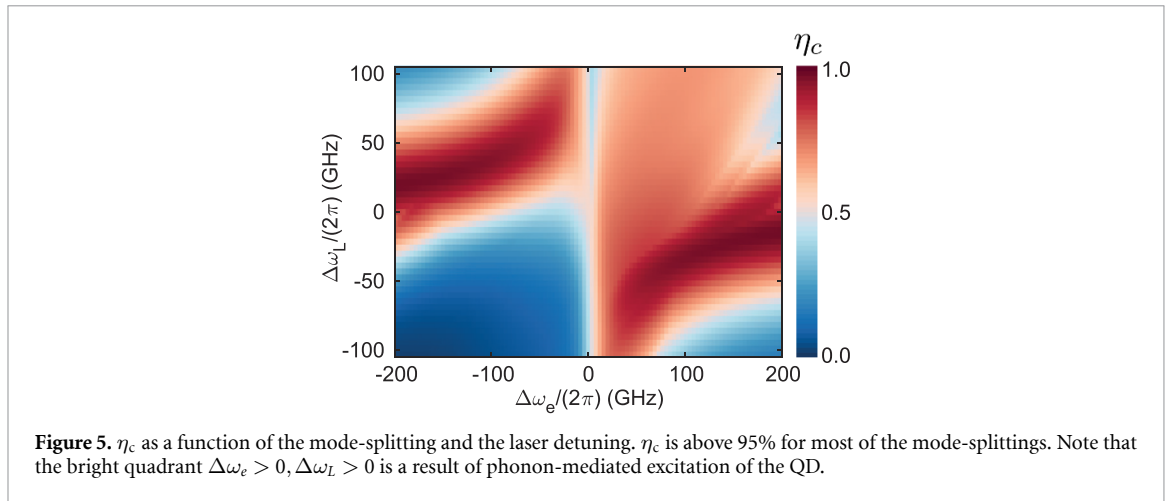
We use our model to map out π_e as a function of the laser detuning, using the parameters following modeling of the data in figure 2. Figure 3(a) shows the behaviour of an ideal (phonon-less) QD in the ‘blue’ collection case. Near-unity population inversion is observed over a range of laser detunings. For a phonon-less QD coupled to the red-detuned cavity mode (‘red’ collection case), this plot would be mirrored with respect to $\Delta\omega_L = 0$. Figures 3(b) and c show the population inversion including the interaction with phonons. The effect of phonons is visible in the striking difference between these two plots and figure 3(a). Despite the asymmetric behaviour between ‘blue’ and ‘red’ collection modes, these results clearly demonstrate that near-unity population inversion can be obtained in both cases, and that the maximum



population inversion is not obtained under strict resonant conditions in this cavity-mediated excitation scheme.

The success of the theory allows us to predict the behaviour on changing the mode-splitting ($\Delta\omega_e/(2\pi)$) over a wide range. Calculating η_c is crucial, as β_c depends on $\Delta\omega_e/(2\pi)$: at small $\Delta\omega_e/(2\pi)$, the two cavity modes overlap, reducing β_c . Figure 5 shows the maximum attainable η_c for a range of laser detunings. The plot confirms that the highest η_c for a finite $\Delta\omega_e$ is achieved away from the strict resonance condition (i.e. $\Delta\omega_L \neq 0$ and $\text{sign}(\Delta\omega_e) = -\text{sign}(\Delta\omega_L)$). The optimum laser frequency approaches the resonance of the QD as the mode-splitting increases. While near-unity efficiency is possible over a large range of mode-splittings, the photon creation efficiency shows a minimum of 50% around $\Delta\omega_e = 0$ as in this case, the QD couples to both cavity modes.

Finally, it is worth considering the input power needed for cavity-mediated excitation of a QD. For the parameters in figure 3, the intra-cavity input pulse area for optimal efficiency is 5.4π . This is less than the pulse area required using the phonon-assisted excitation mechanism. Furthermore, the intra-cavity field is enhanced by the high finesse of the cavity, $E_c = \sqrt{2F/\pi}E_{\text{in}}$ (not included in equation (2)). In our



experiment, we used a one-sided cavity with a finesse of 500, providing an enhancement of 18 in the amplitude of the field.

5. Conclusions

We consider the excitation of a QD via a cavity mode and show that the cavity acts as a dispersive filter, modifying the spectral configuration of the laser pulse. The excitation of the QD proceeds via an indirect route on the Bloch sphere. Nevertheless, a population inversion as high as 98% can be achieved.

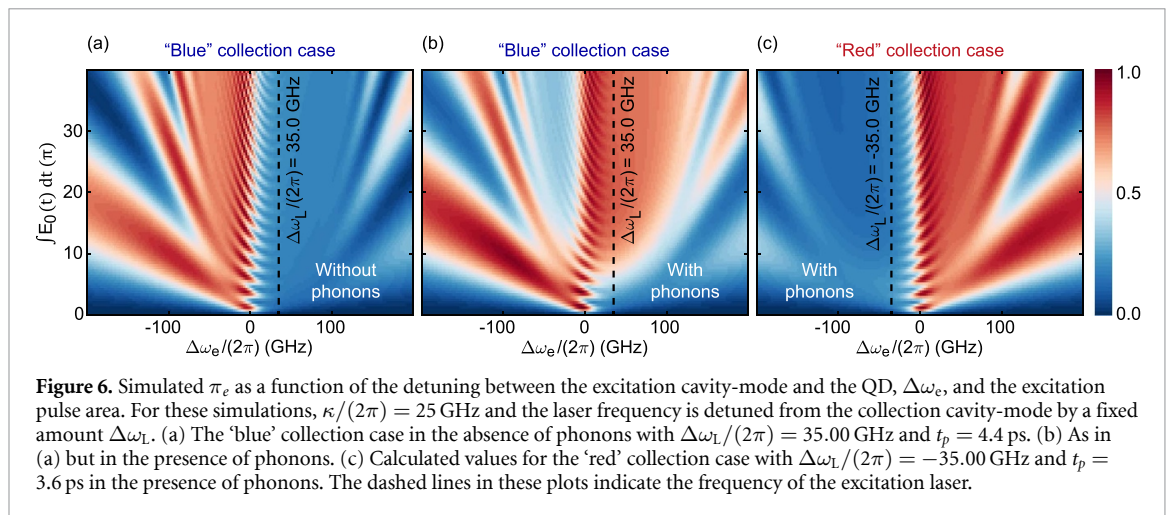
Both the ‘red’ and ‘blue’ collection cases yield equivalent population inversions under optimal parameters. In the ‘red’ case, the excitation mechanism resembles a rapid adiabatic passage scheme in that there is a near-unity plateau for increasing laser powers. This behaviour could be exploited to generate single photons with low sensitivity to fluctuations in the excitation power. In both ‘red’ and ‘blue’ cases, the population inversion is maximum for a laser-pulse detuned with respect to the QD, illustrating the importance of a complete model of the QD-cavity system and its phonon environment to optimize the performance.

Our findings demonstrate that the cavity-mediated excitation of a QD can deliver the high single-photon efficiencies required for optical quantum technologies. The methods developed in this work can be readily applied to a host of different emitter and cavity systems, supporting future advances in solid-state quantum light sources. We comment on a potential drawback for the cavity-based excitation mechanism, namely that the long-lived intra-cavity field may lead to double-excitation events [22, 23]. In this case, the large-bandwidth first photon is filtered away by the cavity; the resultant time jitter on the second photon compromises the indistinguishability of the photons. This problem can be mitigated by choosing $\kappa \gg \Gamma$, where Γ is the lifetime of the TLS in the cavity, a limit appropriate to the experiments performed here.

6. Supplementary

6.1. η_c versus the mode-splitting of the cavity

We map out π_e as a function of the frequency splitting between the excitation and the collection cavities. Figure 6(a) shows the response of an ideal QD (no phonons) as a function of the amplitude of the input field and the mode-splitting of the cavity for a QD-laser detuning of $\Delta\omega_L/(2\pi) = 35$ GHz. High π_e is possible for two laser detunings, the range around zero, and the range around -60 GHz. The first range is disadvantageous as the QD will couple to both cavity modes such that a significant fraction of the photons will be emitted into the excitation cavity. The range around -60 GHz is more useful as the detuning between the excitation cavity and the QD reduces the coupling to the excitation cavity. Figures 6(b) and (c) show π_e for a QD taking into account the effect of phonons for the ‘blue’ and ‘red’ cases. As evident from these plots, π_e is a weak function of the choice, ‘red’ or ‘blue’, and a high photon creation efficiency of the QD is possible for a range of laser detunings.



Data availability statement

The data cannot be made publicly available upon publication because they are not available in a format that is sufficiently accessible or reusable by other researchers. The data that support the findings of this study are available upon reasonable request from the authors.

Acknowledgment

We acknowledge financial support from Swiss National Science Foundation project 200020_204069, Horizon-2020 FET-Open Project QCLUSTER and NCCR QSIT. A J acknowledges support from the European Unions Horizon 2020 Research and Innovation Programme under Marie Skłodowska-Curie Grant Agreement No. 840453 (HiFig), and Research Fund of the University of Basel. A J B gratefully acknowledges support from the EPSRC (UK) Quantum Technology Fellowship EP/W027909/1. S R V, R S, A L and A D W gratefully acknowledge support from DFH/UFA CDFA05-06, DFG TRR160, DFG Project 383065199 and BMBF Q Link X.

ORCID iDs

Alisa Javadi <https://orcid.org/0000-0002-8833-0738>
 Natasha Tomm <https://orcid.org/0000-0002-7508-2261>
 Nadia O Antoniadis <https://orcid.org/0000-0002-6683-8637>
 Alistair J Brash <https://orcid.org/0000-0001-5717-6793>
 Andreas D Wieck <https://orcid.org/0000-0001-9776-2922>
 Arne Ludwig <https://orcid.org/0000-0002-2871-7789>
 Richard J Warburton <https://orcid.org/0000-0002-3095-3596>

References

- [1] Gimeno-Segovia M, Shadbolt P, Browne D E and Rudolph T 2015 *Phys. Rev. Lett.* **115** 020502
- [2] Lo Piparo N, Hanks M, Gravel C, Nemoto K and Munro W J 2020 *Phys. Rev. Lett.* **124** 210503
- [3] Vagov A, Croitoru M D, Axt V M, Kuhn T and Peeters F M 2007 *Phys. Rev. Lett.* **98** 227403
- [4] Ramsay A J, Godden T M, Boyle S J, Gauger E M, Nazir A, Lovett B W, Fox A M and Skolnick M S 2010 *Phys. Rev. Lett.* **105** 177402
- [5] Schupp J, Krcmarsky V, Krutyanskiy V, Meraner M, Northup T and Lanyon B 2021 *PRX Quantum* **2** 020331
- [6] Meraner M, Mazloom A, Krutyanskiy V, Krcmarsky V, Schupp J, Fioretto D A, Sekatski P, Northup T E, Sangouard N and Lanyon B P 2020 *Phys. Rev. A* **102** 052614
- [7] Ates S, Ulrich S M, Ulhaq A, Reitzenstein S, Löffler A, Höfling S, Forchel A and Michler P 2009 *Nat. Photon.* **3** 724
- [8] Thomas S et al 2021 *Phys. Rev. Lett.* **126** 233601
- [9] Gustin C and Hughes S 2020 *Adv. Quantum Technol.* **3** 1900073
- [10] Cosacchi M, Ungar F, Cygorek M, Vagov A and Axt V M 2019 *Phys. Rev. Lett.* **123** 017403
- [11] Huber T, Davanco M, Müller M, Shuai Y, Gazzano O and Solomon G S 2020 *Optica* **7** 380–5
- [12] Kuhlmann A V, Houel J, Brunner D, Ludwig A, Reuter D, Wieck A D and Warburton R J 2013 *Rev. Sci. Instrum.* **84** 073905
- [13] Wang H et al 2019 *Nat. Photon.* **13** 770–5
- [14] Tomm N et al 2021 *Nat. Nanotechnol.* **16** 399–403
- [15] Frey J A, Sniijders H J, Norman J, Gossard A C, Bowers J E, Löffler W and Bouwmeester D 2018 *Opt. Lett.* **43** 4280–3
- [16] Tomm N, Korsch A R, Javadi A, Najer D, Schott R, Valentin S R, Wieck A D, Ludwig A and Warburton R J 2021 *Phys. Rev. Appl.* **15** 054061

- [17] Wei Y J *et al* 2014 *Nano Lett.* **14** 6515–9
- [18] Wu Y, Piper I M, Ediger M, Brereton P, Schmidgall E R, Eastham P R, Hugues M, Hopkinson M and Phillips R T 2011 *Phys. Rev. Lett.* **106** 067401
- [19] Liu F, Martins L M P, Brash A J, Barth A M, Quilter J H, Axt V M, Skolnick M S and Fox A M 2016 *Phys. Rev. B* **93** 161407
- [20] Kaldewey T, Lüker S, Kuhlmann A V, Valentin S R, Chauveau J M, Ludwig A, Wieck A D, Reiter D E, Kuhn T and Warburton R J 2017 *Phys. Rev. B* **95** 241306
- [21] Quilter J H, Brash A J, Liu F, Glässl M, Barth A M, Axt V M, Ramsay A J, Skolnick M S and Fox A M 2015 *Phys. Rev. Lett.* **114** 137401
- [22] Fischer K A, Hanschke L, Wierzbowski J, Simmet T, Dory C, Finley J J, Vučković J and Müller K 2017 *Nat. Phys.* **13** 649–54
- [23] Das S, Zhai L, Čepulskovskis M, Javadi A, Mahmoodian S, Lodahl P and Sørensen A S 2019 arXiv:1912.08303
- [24] Redfield A 1965 The theory of relaxation processes *Advances in Magnetic and Optical Resonance* vol 1 (Academic)
- [25] Breuer H P and Petruccione F 2002 *The Theory of Open Quantum Systems* (Oxford University Press)
- [26] Ardelt P L *et al* 2014 *Phys. Rev. B* **90** 241404
- [27] Johansson J, Nation P and Nori F 2012 *Comput. Phys. Commun.* **183** 1760–72
- [28] Johansson J, Nation P and Nori F 2013 *Comput. Phys. Commun.* **184** 1234–40
- [29] Nazir A and McCutcheon D P 2016 *J. Phys.: Condens. Matter* **28** 103002